OPEN ACCESS
Journal of Multidisciplinary Applied Natural Science Vol. xx No. xx (xxxx) https://doi.org/10.47352/jmans.2774-3047.371
Check for updates
Research Article

Hierarchical NiO/TiO_2-Biomass-Derived Porous Carbon Composite with Improved Electrochemical Kinetics for Energy Storage Applications

Muhammad Nurdin*, Maulidiyah Maulidiyah, Abdul Haris Watoni, Muhammad Zakir, Muliadi Muliadi, Muhammad Zakir Muzakkar, Khusnul Ulul Azmi, Muh Edihar, and Ahmad Zulfan

Received : December 22, 2025	Revised : February 12, 2026	Accepted : February 13, 2026	Online : March 12, 2026

Abstract
The development of high-performance and sustainable anode materials remains a crucial challenge for next-generation energy storage systems. In this study, NiO/TiO_2–biomass-derived porous carbon (BPC) composites were successfully synthesized using palm kernel shell-derived porous carbon as a conductive matrix. Structural and morphological characterizations confirmed the homogeneous distribution of NiO and TiO_2 crystals within the porous carbon framework. The FTIR and XRD analyses verified the presence of metal-oxygen bonds and high phase purity, while SEM revealed a well-developed porous structure. Electrochemical evaluations were performed in KOH solution using a three-electrode configuration. The optimized NiO-TiO_2/BPC (1:2) electrode delivered a specific capacity of 7.76 mAh g^{-1} at 10 mV s^{-1} and sustained 3.59 mAh g^{-1} at 80 mV s^{-1}, demonstrating favorable rate capability. Galvanostatic charge-discharge measurements further confirmed the improved performance, reaching 8.75 mAh g^{-1} at 3 A g^{-1}. This enhanced electrochemical behavior is attributed to the synergistic integration of conductive porous carbon with electroactive NiO and TiO_2 phases. These findings indicate that the NiO-TiO_2/BPC composite functions as a hybrid alkaline electrode material and has potential for safe and sustainable aquatic energy storage devices.

Keywords: biomass-derived porous carbon, NiO–TiO_2/BPC composite, aqueous alkaline, hybrid electrode system, energy storage

1. INTRODUCTION

To date, research on nickel-based materials has made significant progress, especially in the electrochemical performance of nickel in energy storage devices. Among metal oxide molecules, nickel oxide (NiO) exhibits a reversible redox reaction in alkaline media, providing a significant Faradaic contribution to charge storage [1]. However, in practice, NiO exhibits a low specific capacitance, well below its theoretical value (2584 F g^{-1}). This is generally due to the structural limitations of single transition metal oxides [2]. One effort that is still under development is a mixture of transition-metal oxides.

As a single crystal material, titanium dioxide (TiO_2) has a high energy density of 9.6 W·h·kg^{-1} and excellent chemical stability [2]. However, intrinsically, pure TiO_2 has very low electrical conductivity (<10^{-10} S·cm^{-1}) due to its semiconducting nature, although this value can be improved by modifying or compositing it with dopants [3]. For example, a two-electrode array of NiO-TiO_2 yields a significant energy density of 54.29-4446 W·kg^{-1} with high power density, as well as competent cyclic stability after 10,000 cycles [4]. This improvement occurs because the hierarchical NiO/TiO_2 core exhibits enhanced pseudocapacitive behavior, driven by the synergistic effect of the co-encapsulation of TiO_2 and NiO [5]. In addition, the appropriate composition of NiO dopants in TiO_2 can increase the electrical conductivity up to 1.7 times that of pure TiO_2, which is about 4.92 × 10^{-5} S·cm^{-1} [6]. Thus, TiO_2 can be used as a potential electrode material for energy storage devices [7]–[9].

On the other hand, the combination of transition metals and carbon has also been reported as a hybrid composite designed to provide high energy and power density along with high rate capability and cyclic stability. Thanks to its porous architecture, high surface area, and interconnected pore network, carbon provides efficient electron transport pathways, readily accessible surfaces, and shorter ion-diffusion distances [10]. These features are highly advantageous in energy storage systems, where fast ion transport is crucial for high-rate

Please cite this article as: M. Nurdin, M. Maulidiyah, A. H. Watoni, M. Zakir, M. Muliadi, M. Z. Muzakkar, K. U. Azmi, M. Edihar, and A. Zulfan. (2026). "Hierarchical NiO/TiO2-Biomass-Derived Porous Carbon Composite with Improved Electrochemical Kinetics for Energy Storage Applications". *Journal of Multidisciplinary Applied Natural Science*. https://doi.org/10.47352/jmans.2774-3047.371

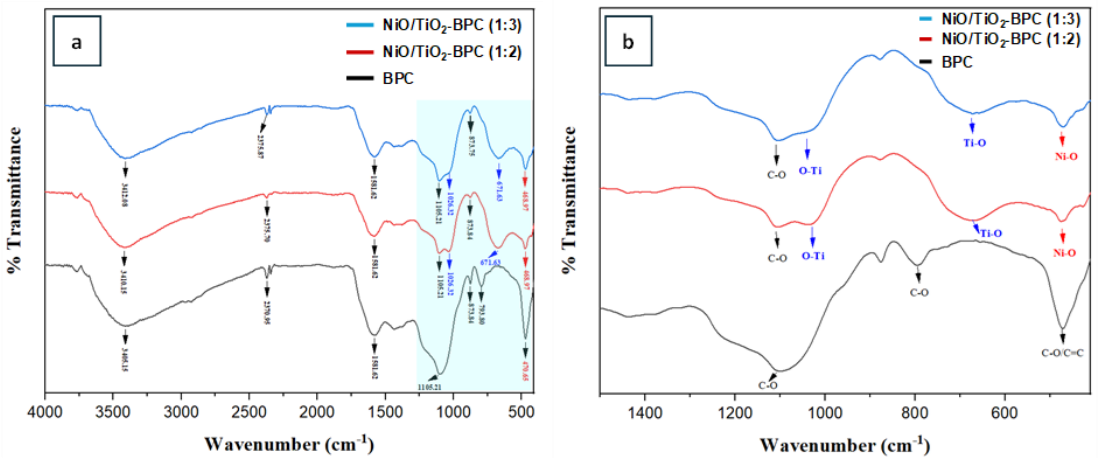

Figure 1. FTIR Spectra of (a) BCP and NiO/TiO_2-BPC; (b) C–O, Ti–O and Ni–O.

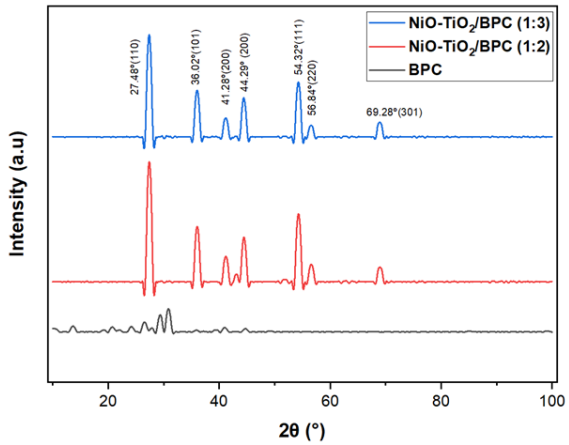

Figure 2. XRD patterns of BPC and NiO-TiO_2/BPC composites.

performance. For example, a C-TiO_2 composite successfully prepared via a hydrothermal method is capable of improving the electrochemical performance [11] and the charging capacity up to 500 mAh g^{-1}, greater than the theoretical capacity of TiO_2 (335 mAh g^{-1}) and C (372 mAh g^{-1}) [6] [12].

Based on the above findings, the use of biomass-derived porous carbon as a conductive support for NiO–TiO_2 composites in aqueous alkaline electrolyte systems remains relatively limited, especially in studies that examine the role of the oxide–carbon composition ratio on structural characteristics, morphology, and charge storage mechanisms. In line with this, extrinsic cation interactions in aqueous alkaline electrolytes and their effects on the electrochemical characteristics and activities of composite hybrid electrodes have been widely studied [13]–[15]. For example, the interaction between metal oxide and C in aqueous electrolytes, especially potassium hydroxide (KOH), exhibits a synergistic effect, leading to improved electrochemical kinetics and increased charge storage capacity [16]–[19]. Based on these considerations, this study reports the synthesis and characterization of NiO–TiO_2/BPC hybrid composites with varying mass ratios, designed as battery-type electrodes for KOH-based aqueous alkaline energy storage systems.

2. MATERIALS AND METHODS

2.1. Materials

Palm shell waste was used as the biomass precursor for porous carbon synthesis. Nickel(II) nitrate hexahydrate ($Ni(NO_3)_2 \cdot 6H_2O$, 99%) and ammonium hydroxide (NH_4OH, 25%) were employed as nickel sources and precipitating agents, respectively. Commercial TiO_2 (Degussa P25) was used without further purification. KOH (85%) served as the chemical activating agent, while hydrochloric acid (HCl, 37%) was used for

post-activation washing. Isopropanol (C_3H_8O, 99.5%), polyethylene glycol (PEG, average Mw 400), and Triton™ X-100 were used as solvents and surfactants during nanocomposite preparation. Ethanol (C_2H_5OH, 99.8%) was utilized for composite dispersion. All reagents were of analytical grade and used as received. Deionized water was used throughout the experiments. High-purity nitrogen gas (N_2) was employed to maintain an inert atmosphere during thermal treatments. For electrochemical measurements, a 2 M KOH aqueous solution was used as the electrolyte, with Ag/AgCl and platinum wire serving as the reference and counter electrodes, respectively.

2.2. Methods

2.2.1. Preparation of Biomass-Derived Porous Carbon (BPC)

Palm shell waste was thoroughly washed with deionized water and oven-dried at 110 °C. The dried biomass was cut into small pieces and pre-carbonized at 400 °C for 4 h. The resulting carbon was ground and sieved through a 400-mesh sieve to obtain a uniform powder. Chemical activation was performed by impregnating the carbonized powder with a KOH solution at a mass ratio of carbon to KOH of 1:5. The mixture was magnetically stirred for 12 h to ensure homogeneous impregnation, followed by filtration and drying at 110 °C for 1 h. The dried sample was then heated under a nitrogen atmosphere at a heating rate of 5 °C min^{-1} up to 800 °C and maintained for 2.5 h. After cooling to room temperature, the activated carbon was washed repeatedly with 1 M HCl until a neutral pH was achieved to remove residual inorganic species. The final product was dried at 105 °C and denoted as biomass-derived porous carbon (BPC).

2.2.2. Synthesis of NiO-TiO_2 Composite

The $Ni(NO_3)_2 \cdot 6H_2O$ was dissolved in a mixed solvent consisting of 20 mL isopropanol and 20 mL polyethylene glycol (PEG) under continuous magnetic stirring for 24 h to obtain a homogeneous solution. NH_4OH was then added dropwise until the solution reached pH 11. Subsequently, 10 mL of Triton™ X-100 was introduced to suppress particle agglomeration. The mixture was gradually heated to 80 °C, followed by the addition of pre-calcined TiO_2. The resulting gel was dried at 200 °C and then calcined at 500 °C to obtain the NiO–TiO_2 nanocomposite.

2.2.3. Synthesis of NiO-TiO_2/Biomass-Derived Porous Carbon (BPC) Composite

NiO-TiO_2/BPC composites were prepared by physically mixing NiO/TiO_2 nanocomposites with BPC at a mass ratio of 1:3 and 1:2 (wt%). The mixture was dissolved in 50 mL of deionized water and then ultrasonicated for 1 hour. The suspension mixture was then transferred to a 100 mL Teflon-lined stainless-steel autoclave at 200 °C for 6 h. After the reaction was completed, the autoclave was left at room temperature, the obtained product was washed several times with deionized water and ethanol, then dried at 60 °C for 24 h. Next, the obtained product was calcined at 350 °C for 2 h. Then, prepare the electrode by homogenizing a

Table 1. The average crystallite sizes of BPC and NiO-TiO_2/BPC.

Material	2θ (°)	FWHM	Size (nm)
BPC	26.62	0.8141	10.02
	29.36	0.7574	10.84
	30.86	1.0059	8.19
NiO-TiO_2/BPC	27.48	0.78672	10.39
	36.02	0.78221	10.67
	41.37	0.78537	10.80
	44.43	0.77167	11.12
	54.32	0.78363	11.39
	56.84	0.77711	11.60
	69.28	0.81290	11.85

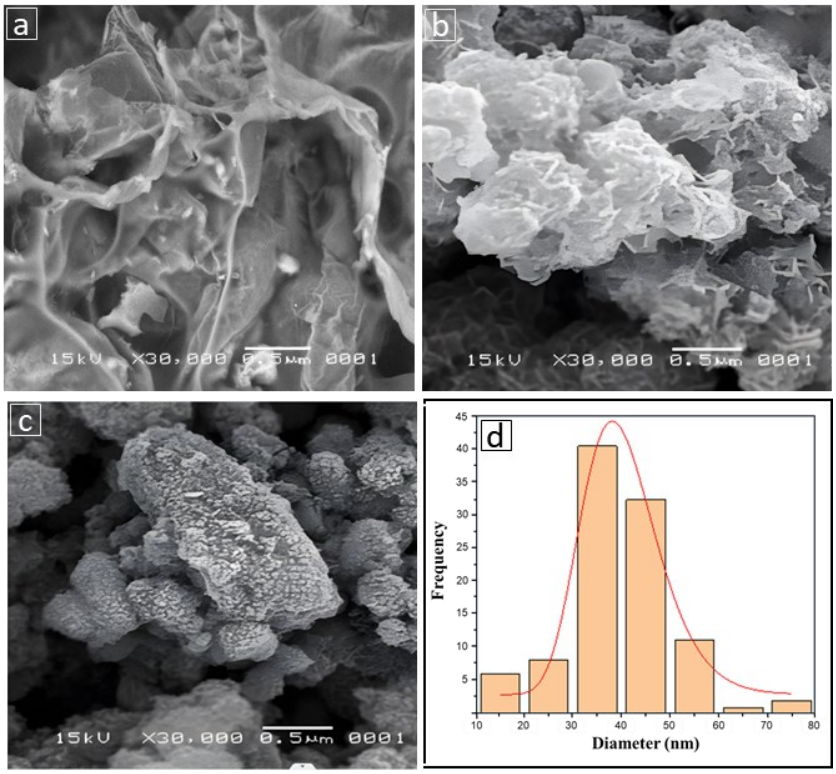

Figure 3. SEM morphology of (a) BPC, (b) NiO-TiO_2/BPC (1:2), (c) NiO-TiO_2/BPC (1:3), and (d) the pore size distribution of BPC.

mixture of 0.05 g of NiO-TiO_2/BPC nanocomposite and 0.3 g of paraffin oil stirred at 400 rpm for 15 min while heating at 80 °C. Finally, the NiO-TiO_2/BPC paste was placed into a 3 mm diameter glass tube, gently pressed, smoothed, and connected to a copper wire.

2.2.4. Characterizations

Characterization of NiO-TiO_2/BPC composite using Xray diffraction, XRD (Shimadzu 6000) at 2θ=20-80° with Cu-Ka= 1.54060). The morphology of the nanocomposites was characterized using scanning electron microscopy, SEM (HITACHI SU3500). To identify chemical bonds and functional groups, Fourier transforms infrared (FT-IR) spectra was used (Shimadzu Varian 4300 spectrophotometer). The electrochemical properties of the nanocomposites were characterized by cyclic voltammetry techniques using a DY2100 potentiostat.

2.2.5. Computational Image Analysis

SEM images of BPC were processed using ImageJ software (J904 Beta) to qualitatively evaluate pore size distribution. The analysis involved applying the built-in smoothing function to reduce image noise, followed by manual adjustment of the threshold to distinguish pore regions from the carbon matrix. The images were then converted into binary format, and particle analysis routines were executed to estimate pore size features. This image-based analysis was employed solely to provide morphological insights into the pore structure and was not intended as a quantitative substitute for gas adsorption measurements.

2.2.6. Electrochemical Kinetics Evaluation

Cyclic voltammetry (CV) measurements were carried out using a three-electrode electrochemical system. The NiO-TiO_2/BPC composite and BPC electrodes were employed as the working electrodes, while an Ag/AgCl electrode and a platinum wire served as the reference and counter electrodes, respectively. All electrochemical tests were conducted in 2 M KOH aqueous solution as the supporting electrolyte. CV curves were recorded within a potential window of -0.1–0.6 V (vs. Ag/AgCl) at a scan rate of 0.1 V s^{-1} at room temperature. Galvanostatic charge–discharge

(GCD) tests were performed using a LAND battery testing system within a voltage range of 0.01–3.0 V at room temperature. The electrochemical performance of the NiO/TiO_2–BPC composite electrodes was evaluated under various current densities to investigate their charge storage behavior and cycling stability.

3. RESULTS AND DISCUSSIONS

3.1. FTIR Spectra of BCP and NiO-TiO_2/BPC Composites

Figure 1(a–b) presents the FTIR spectra of pristine BPC and NiO-TiO_2/BPC composites. The broad band at 3410 cm^{-1} is attributed to O–H stretching vibrations from surface hydroxyl groups and adsorbed moisture [20], while the weak absorption around 2735 cm^{-1} corresponds to C–H stretching vibrations of residual aliphatic groups in the biomass-derived carbon [21]. The band at 1581 cm^{-1} is associated with C=O stretching or O–H bending vibrations of oxygen-containing functional groups [22]. In the low-wavenumber region, the bands observed at 1105–1206 cm^{-1} are assigned to C–O stretching [23], indicating the preservation of oxygenated carbon functionalities after composite formation. Distinct absorption bands at 671 and 468 cm^{-1} are attributed to Ti–O [24][25] and Ni-O [26], stretching vibrations, respectively, consistent with reported FTIR spectra of TiO_2 and NiO.

3.2. XRD Patterns of BPC and NiO-TiO_2/BPC Composites

Figure 2 displays the XRD patterns of pure BPC and the NiO–TiO_2/BPC composite. The BPC sample exhibits a broad diffraction band centered at 2θ = 24–30°, which is characteristic of predominantly amorphous carbon. After the incorporation of NiO–TiO_2, distinct and sharp diffraction peaks appear, indicating the formation of a well-crystallized oxide phase on the carbon framework. The observed diffraction peaks at 2θ = 27.48°, 36.02°, 41.37°, 54.32°, 56.84°, and 69.28° can be consistently indexed to the (110), (101), (200), (111), (220), and (301) crystallographic planes of rutile TiO_2, respectively, in full agreement with JCPDS Card No. 21-1276 [27][28]. Within the detection limits of the XRD instrument, no characteristic reflections corresponding to anatase TiO_2 (e.g., ~25.3°, 37.8°, 48.0°, JCPDS No. 21-1272) were observed, indicating that the TiO_2 phase in the composite is predominantly rutile. Therefore, our phase identification is based strictly on crystallographic matching with standard JCPDS reference patterns, not on the inferred phase transformation mechanism. A diffraction peak centered at 2θ = 44.63° was detected in the composite sample. Although this region may

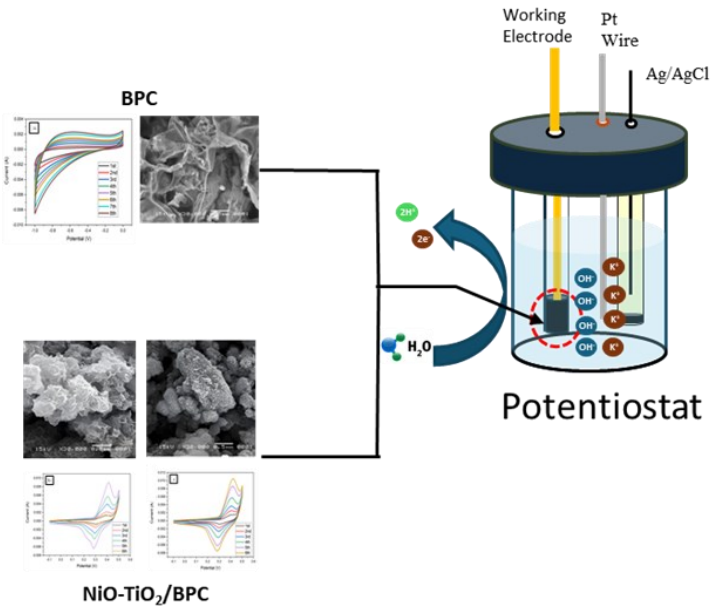

Gambar 4. Electrochemical evaluations were performed in KOH solution using a three-electrode configuration.

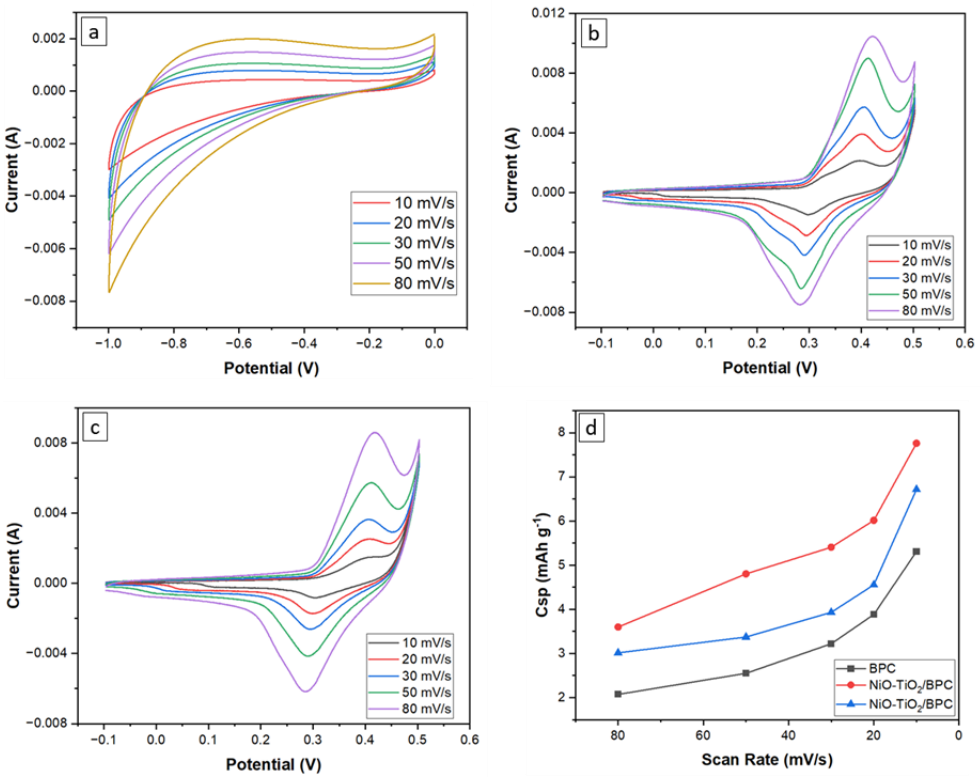

Figure 5. Voltamogram of (a) BPC, (b) NiO-TiO_2/BPC (1:2), (c) NiO-TiO_2/BPC (1:3), and (c) Csp of BPC and NiO-TiO_2/BPC.

overlap with reflections from NiO and metallic Ni, the absence of additional diagnostic metallic Ni peaks at 51.8° (200) and 76.4° (220) (JCPDS Card No. 03-1051) [29], combined with the oxidative calcination atmosphere used during the synthesis, strongly suggests the absence of crystalline metallic Ni. In contrast, the observed reflections are fully consistent with cubic NiO (JCPDS Card No. 04-0835) [29], confirming that the nickel is predominantly present in the oxidized state.

The average crystallite sizes of BPC and NiO-TiO_2/BPC were calculated from the XRD patterns using the Debye-Scherrer as shown as Equation 1;

$$D = \frac{k\lambda}{\beta\cos\theta} \quad (1)$$

where D is the average crystallite size, k is a dimensionless shape factor with a value near unity (0.9), λ is the X-ray wavelength (0.15406), β is the full width at half maximum (FWHM), and θ is the Bragg angle [30]. As presented in Table 1, the average crystallite sizes for BPC and NiO/TiO_2-BPC were found to be in the range of 9.19–10.02 and 10.39–11.85 nm, respectively.

3.3. SEM Morphology of BCP and NiO-TiO_2/BPC Composites

Figure 3(a) presents the SEM image of biomass-derived porous carbon (BPC). The BPC exhibits a rough surface morphology with an irregular, highly developed pore network, characteristic of chemically activated carbon produced via KOH activation [31]. The presence of interconnected pores suggests the formation of a hierarchical porous framework that facilitates electrolyte penetration and ion transport.

Upon incorporation of NiO–TiO_2, noticeable morphological differences are observed depending on the composite ratio. The NiO–TiO_2/BPC (1:2) sample (Figure 3(b)) displays a relatively dense oxide coverage, where portions of the carbon pore structure appear partially filled by aggregated oxide particles. In contrast, the NiO–TiO_2/BPC (1:3) composite (Figure 3(c)) shows a more homogeneous dispersion of oxide nanoparticles over the carbon scaffold while maintaining visible pore accessibility. This indicates that the oxide-to-carbon ratio plays a critical role in balancing active redox sites and electrolyte-accessible surface area.

The pore size distribution of BPC, shown in

Figure 3(d), was estimated from SEM micrographs of the thin-layer sample using the particle analysis function in ImageJ software. The observed pore features predominantly fall within the 20–80 nm range, corresponding to mesoporous structures. These dimensions are larger than the crystallite sizes derived from XRD using the Debye–Scherrer equation (Table 1); however, this difference is expected and not contradictory. Crystallite size reflects the coherent diffraction domain of crystalline phases, whereas SEM-observed pore features represent inter-aggregate voids within the carbon framework. Therefore, the two parameters describe distinct structural characteristics and should not be directly equated.

3.4. Electrochemical Kinetics Evaluation of BCP and NiO/TiO_2-BPC Composites

The electrochemical performance test of BCP and NiO/TiO_2-BPC Composite was carried out using a three-electrode system as seen in Figure 4. The electrochemical characteristics of the BPC and NiO–TiO_2/BPC composite electrodes were evaluated by CV in 2 M KOH within a potential window of -0.1 to 0.6 V (vs. Ag/AgCl) at scan rates ranging from 10 to 80 mV s^{-1}, as presented in Figures 5(a–c). All electrodes exhibited progressively increased current response with increasing scan rate, indicating stable electrochemical behavior and reasonably fast charge-transfer kinetics in the aqueous alkaline system [32]. The CV curves of the BPC electrode exhibit a quasi-rectangular profile without well-defined redox peaks, characteristic of charge storage dominated by electric double-layer capacitance (EDLC) at the carbon–electrolyte interface. In contrast, the NiO–TiO_2/BPC composites exhibit noticeable deviations from the ideal EDLC shape, characterized by broadened redox humps and enhanced current response. This behavior suggests the presence of additional surface -controlled Faradaic reactions associated with valence-state transitions of nickel species under alkaline conditions. Importantly, the electrochemical features do not resemble bulk conversion reactions typical of lithium-ion battery systems but they are more consistent with surface pseudocapacitive processes operating within an aqueous alkaline hybrid configuration.

Determination of specific capacitance (Csp) is done using the following Equation 2. Plot the current (I) against the potential (V) and identify the relevant area under the curve (reduction or oxidation region). Then, integrate the current with respect to potential to obtain the charge (Q), Equation 3.

Tabel 2. Specific capacitance performance of BPC and NiO/TiO_2–BPC electrodes.

Electrode	Scan rate (mV/s)	Area	Massa (g)	ΔV (A)	Q (C g^{-1})	Csp (mAh g^{-1})
BPC	10	0.00095566	0.005	1	19.11	5.31
	20	0.00139751	0.005	1	13.97	3.89
	30	0.00173831	0.005	1	11.58	3.22
	50	0.00229526	0.005	1	9.18	2.55
	80	0.00298461	0.005	1	7.46	2.07
NiO-TiO_2/BPC (1:2)	10	0.00083814	0.005	0.6	27.93	7.76
	20	0.00129885	0.005	0.6	21.64	6.01
	30	0.00175182	0.005	0.6	19.46	5.40
	50	0.00259268	0.005	0.6	17.28	4.80
	80	0.00310817	0.005	0.6	12.95	3.59
NiO-TiO_2/BPC (1:3)	10	0.00072516	0.005	0.6	24.17	6.71
	20	0.00098379	0.005	0.6	16.39	4.55
	30	0.00127333	0.005	0.6	14.14	3.93
	50	0.00182101	0.005	0.6	12.14	3.37
	80	0.00260403	0.005	0.6	10.85	3.01

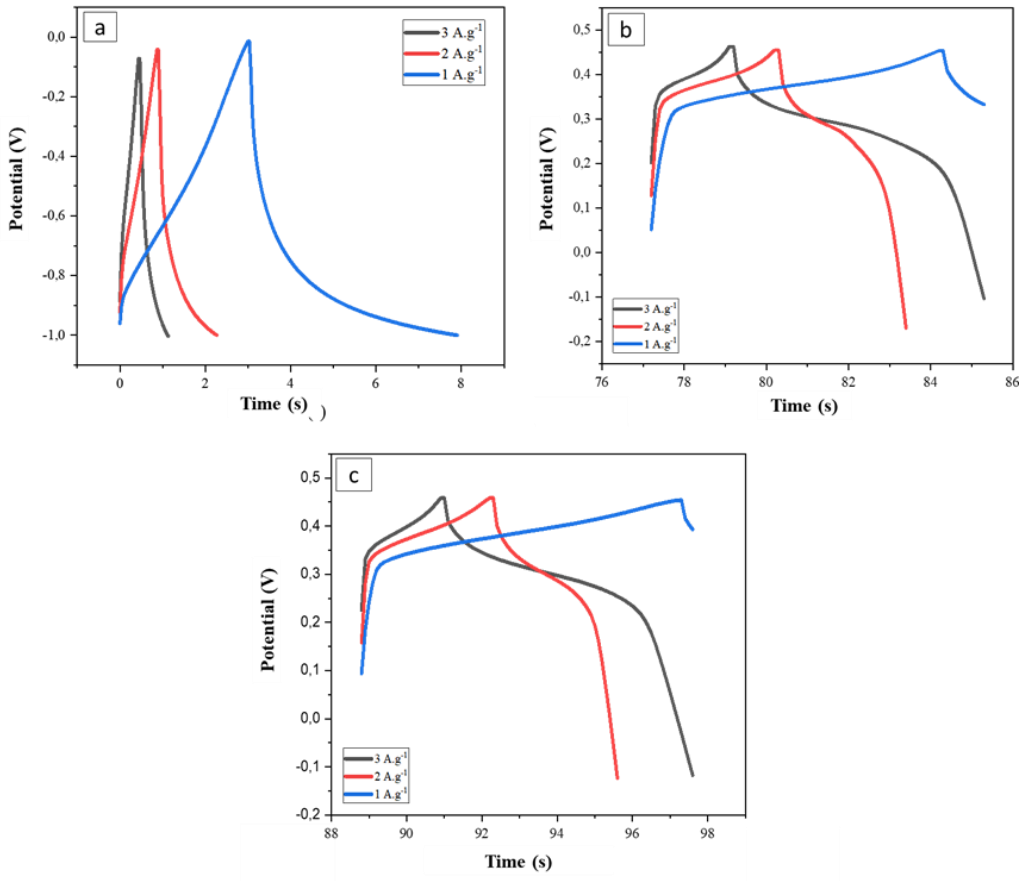

Figure 6. Galvanostatic charge–discharge (GCD) profiles of the electrodes: (a) BPC, (b) NiO/TiO_2–BPC (1:2), and (c) NiO/TiO_2–BPC (1:3).

$$Q = \int_{V_1}^{V_2} I(V)dV \quad (2)$$

$$C_{sp} = \frac{Q(C)}{3.6\ x\ m} \quad (3)$$

where m is the mass (in grams), and the factor 3.6 is used to convert Coulombs to milliampere-hours (mAh).

Figure 5(d) and Table 2 summarize the specific capacitance values of the BPC and NiO-TiO_2/BPC electrodes, calculated from cyclic voltammetry curves at various scan rates. Based on the recalculated specific capacitance results summarized in Table 2, the BPC electrode exhibits a Csp value of 5.31 mAh g^{-1} at a scan rate of 10 mV s^{-1}, which then decreases gradually to 2.07 mAh g^{-1} at 80 mV s^{-1}. In contrast, the NiO–TiO_2/BPC composite electrode exhibits a significant increase in specific capacitance across all scan rates. The NiO–TiO_2/BPC (1:2) electrode produced the highest Csp value, which was 7.76 mAh g^{-1} at 10 mV s^{-1}, followed by 6.01, 5.41, 4.80, and 3.60 mAh g^{-1} at scan rates of 20, 30, 50, and 80 mV s^{-1}, respectively. These values were consistently higher than those of both BPC and NiO–TiO_2/BPC (1:3) electrodes. The NiO–TiO_2/BPC (1:3) electrode showed a Csp value of 6.71 mAh g^{-1} at 10 mV s^{-1}, but experienced a sharper decrease to 3.01 mAh g^{-1} at 80 mV s^{-1}. This indicates that increasing the carbon fraction relative to the metal oxide can reduce the number of active redox sites on NiO that contribute to the energy storage mechanism.

The galvanostatic charge–discharge (GCD) profiles in Figure 6 demonstrate the differences in charge storage characteristics between BPC and NiO-TiO_2/BPC composites. The BPC electrode (Figure 6(a)) displays a relatively linear and nearly symmetrical charge-discharge curve, which is typical of the EDLC mechanism due to the adsorption/desorption of OH^- ions on the porous carbon surface. In contrast, the NiO-TiO_2/BPC electrode (Figures 6(b–c)) exhibits a deviation from linearity and a gentler potential slope during the discharge process, indicating the contribution of the electrode surface redox reaction in the KOH

Table 3. Galvanostatic Charge/Discharge (GCD) Data for BPC and NiO/TiO_2–BPC Electrodes.

Material	Energy Density (A g^{-1})	Time ΔV (s)	Mass (g)	Current, I (A)	Capacity, C_{sp} (mAh g^{-1})
CA	3	8.00	0.005	0.015	6.67
	2	2.20	0.005	0.010	1.22
	1	1.13	0.005	0.005	0.31
Ni-TiO_2/CA (1:2)	3	10.50	0.005	0.015	8.75
	2	7.00	0.005	0.010	3.89
	1	10.50	0.005	0.005	2.91
Ni-TiO_2/CA 1:3)	3	8.60	0.005	0.015	7.17
	2	6.70	0.005	0.010	3.72
	1	8.60	0.005	0.005	2.39

medium; thus, the charge storage mechanism is a hybrid (EDLC + surface pseudocapacitive). Quantitatively (Table 3), the NiO-TiO_2/BPC (1:2) composite showed the highest capacity of 8.75 mAh g^{-1} at 3 A g^{-1}, higher than that of BPC (6.67 mAh g^{-1}) and the (1:3) composite (7.17 mAh g^{-1}), which is consistent with the CV results (Table 2 and Figure 5(d)), where the 1:2 ratio also yielded the highest Csp at all scan rates. The decreasing capacity with increasing current density indicates ion-diffusion limitations at high current densities, a common phenomenon in porous electrode systems in aqueous electrolytes [19][33]. Thus, the CV and GCD data consistently confirm that the performance improvement in the 1:2 composite stems from the optimal balance between carbon conductivity and the number of active redox sites of NiO–TiO_2, without involving the bulk conversion mechanism typical of lithium-ion batteries.

4. CONCLUSIONS

In this study, biomass-derived porous carbon (BPC) was successfully integrated with NiO and TiO_2 to form NiO–TiO_2/BPC composites with controlled mass ratios, resulting in structurally stable and electrochemically active hybrid electrodes. XRD analysis confirmed the dominance of the rutile TiO_2 phase alongside oxidized nickel species without evidence of metallic Ni, while SEM observations revealed a hierarchical mesoporous carbon framework (20–80 nm) that remained accessible after oxide incorporation. Electrochemical evaluation in 2 M KOH demonstrated that pristine BPC exhibited typical electric double-layer capacitance behavior, whereas the NiO–TiO_2/BPC composites displayed enhanced charge storage due to the combined contribution of surface-controlled capacitive processes and reversible faradaic reactions in alkaline media. The NiO–TiO_2/BPC (1:2) electrode delivered the highest specific capacity of 7.76 mAh g^{-1} at 10 mV s^{-1} and 8.75 mAh g^{-1} at 3 A g^{-1}, maintaining superior rate performance compared to BPC and the 1:3 composite. These findings indicate that optimizing the oxide-to-carbon ratio is critical to balancing redox-active sites and pore accessibility. Overall, the results demonstrate that NiO–TiO_2/BPC composites function effectively as hybrid

capacitive electrodes in alkaline systems, although further validation in lithium-based electrolytes would be required before considering lithium-ion battery applications.

AUTHOR INFORMATION

Corresponding Author

Muhammad Nurdin — Department of Chemistry, Universitas Halu Oleo, Kendari-93232 (Indonesia); Nickel Research Institute, Universitas Muhammadiyah Kendari, Kendari-93232 (Indonesia);
orcid.org/0000-0002-6727-9283
Email: mnurdin06@yahoo.com

Authors

Maulidiyah Maulidiyah — Department of Chemistry, Universitas Halu Oleo, Kendari-93232 (Indonesia);
orcid.org/0000-0001-5643-9854

Abdul Haris Watoni — Department of Chemistry, Universitas Halu Oleo, Kendari-93232 (Indonesia);
orcid.org/0000-0002-0724-2366

Muhammad Zakir — Department of Chemistry, Hasanuddin University, Makassar-90245 (Indonesia);
orcid.org/0000-0002-2141-5681

Muliadi Muliadi — Department of Chemistry, Universitas Khairun, Ternate-97721 (Indonesia);
orcid.org/0000-0003-2123-7851

Muhammad Zakir Muzakkar — Department of Chemistry, Universitas Halu Oleo, Kendari-93232 (Indonesia);
orcid.org/0000-0002-9749-0637

Khusnul Ulul Azmi — Department of Chemistry, Universitas Halu Oleo, Kendari-93232 (Indonesia);
orcid.org/0009-0002-0996-2225

Muh Edihar — Department of Chemistry, Institut Sains Teknologi dan Kesehatan (ISTEK) 'Aisyiyah Kendari, Kendari-93116 (Indonesia);
orcid.org/0009-0000-9270-2672

Ahmad Zulfan — Department of Environmental Engineering, Universitas Indonesia, Kota Depok-16424 (Indonesia);
orcid.org/0009-0002-5513-7015

Author Contributions

K. U. A. and A. Z. performed all experiments; M. N. coordinated the research; M. E. and M. M. 1. wrote the manuscript; A. H. W., M. Z. and M. Z. M. compiled and processed the research data; M. M. 2. was responsible for proofreading the manuscript. All authors have read and approved the published version of the manuscript.

Conflicts of Interest

The authors declare that there are no conflicts of interest regarding the publication of this paper. The authors affirm that there are no financial, personal, or institutional relationships that could be perceived as influencing the presentation or interpretation of the research findings reported in this manuscript.

ACKNOWLEDGEMENT

We are grateful for financial support from the Ministry of Education, Culture, Research and Technology of the Republic of Indonesia under Fundamental Research Grant No. 014/E5/PG.02.00.PL.BATCH.2/2004 and 149/UN29.20/PG/2024.

DECLARATION OF GENERATIVE AI

During the preparation of this work, the authors used ChatGPT from OpenAI to assist with language refinement and improve the clarity of academic expression. After using this tool, the authors carefully reviewed and edited the content as needed and take full responsibility for the content of the publication.

REFERENCES

[1] H. Moreno Fernández, J. Gallenberger, C. Mempin, I. Khalek, M. Neumann, S. Lotfi, S. M. Kim, M. Li, C. Tian, and J. P. Hofmann. (2024). "Phase Transitions in NiO During the Oxygen Evolution Reaction Assessed via Electrochromic Phenomena through Operando UV–Vis Spectroscopy". *Electrochimica Acta.* **498**. 10.1016/j.electacta.2024.144626.

[2] S. H. S. Pai, S. K. Pandey, E. J. J. Samuel, J. U. Jang, A. K. Nayak, and H. Han. (2024).

"Recent Advances in NiO-Based Nanostructures for Energy Storage Device Applications". *Journal of Energy Storage.* **76**. 10.1016/j.est.2023.109731.

[3] T. Appadurai, C. Subramaniyam, R. Kuppusamy, S. Karazhanov, and B. Subramanian. (2019). "Electrochemical Performance of Nitrogen-Doped TiO2 Nanotubes as Electrode Material for Supercapacitor and Li-Ion Battery". *Molecules.* **24** (16). 10.3390/molecules24162952.

[4] B. S. Harisha, B. Akkinepally, J. Shim, and J. Lim. (2024). "Hybrid NiO@TiO2 Nano-Architecture for Improved Electrochemical Performance with Simulation Corroboration". *Journal of Energy Storage.* **87**. 10.1016/j.est.2024.111466.

[5] T. Azis, L. Ashari, M. Z. Muzakkar, M. Nurdin, L. O. M. Z. Mulkiyan, L. O. A. Salim, M. Edihar, and A. A. Umar. (2024). "Enhancing Cyclic Voltammetry Performance with N-Graphene-Supported Coupled NiO/TiO2 Hollow Nanospheres as Superior Anode Material". *Chemical Papers.* **78** (8): 4719-4731. 10.1007/s11696-024-03408-3.

[6] D. Kang, J. Li, and Y. Zhang. (2020). "Effect of Ni Doping Content on Phase Transition and Electrochemical Performance of TiO2 Nanofibers Prepared by Electrospinning Applied for Lithium-Ion Battery Anodes". *Materials.* **13** (6). 10.3390/ma13061302.

[7] L. Baudino, P. Zaccagnini, S. Bianco, M. Castellino, A. Lamberti, C. F. Pirri, and M. Serrapede. (2024). "Unveiling the Power of Titanium Dioxide for Energy Storage and Electrochemical Technologies". *ChemCatChem.* **17** (4). 10.1002/cctc.202401689.

[8] P. Si, Z. Zheng, Y. Gu, C. Geng, Z. Guo, J. Qin, and W. Wen. (2023). "Nanostructured TiO2 Arrays for Energy Storage". *Materials.* **16** (10). 10.3390/ma16103864.

[9] C. Sippel, W. C. Guaglianoni, and C. P. Bergmann. (2022). In: "Engineering Materials". 73-96. 10.1007/978-3-030-86822-2_5.

[10] P. Sinha, S. Banerjee, and K. K. Kar. (2020). In: "Springer Series in Materials Science". 145-178. 10.1007/978-3-030-52359-6_6.

[11] M. Maulidiyah, T. Azis, L. Lindayani, D. Wibowo, L. O. A. Salim, A. Aladin, and M. Nurdin. (2019). "Sol-Gel TiO2/Carbon Paste Electrode Nanocomposites for Electrochemical-Assisted Sensing of Fipronil Pesticide". *Journal of Electrochemical Science and Technology.* **10** (4): 394-401. 10.33961/jecst.2019.00178.

[12] Z. H. Mahmoud, Y. Ajaj, G. K. Ghadir, H. M. Al-Tmimi, H. H. Jasim, M. Al-Salih, M. H. S. Alubiady, A. M. Al-Ani, S. S. Jumaa, S. Azat, G. F. Smaisim, and E. Kianfar. (2024). "Carbon-Doped Titanium Dioxide (TiO2) as Li-Ion Battery Electrode: Synthesis, Characterization, and Performance". *Results in Chemistry.* **7**. 10.1016/j.rechem.2024.101422.

[13] M. E. G. Lyons, R. L. Doyle, I. Godwin, M. O'Brien, and L. Russell. (2012). "Hydrous Nickel Oxide: Redox Switching and the Oxygen Evolution Reaction in Aqueous Alkaline Solution". *Journal of The Electrochemical Society.* **159** (12): H932-H944. 10.1149/2.078212jes.

[14] M. Natsir, Y. I. Putri, D. Wibowo, M. Maulidiyah, L. O. A. Salim, T. Azis, C. M. Bijang, F. Mustapa, I. Irwan, Z. Arham, and M. Nurdin. (2021). "Effects of Ni–TiO2 Pillared Clay–Montmorillonite Composites for Photocatalytic Enhancement Against Reactive Orange Under Visible Light". *Journal of Inorganic and Organometallic Polymers and Materials.* **31** (8): 3378-3388. 10.1007/s10904-021-01980-9.

[15] T. Azis, M. Z. Muzakkar, A. T. Nurwahida, N. Dali, O. A. Kadir, D. A. Lestari, and O. A. Salim. (2023). "ZnO-Enhanced Reduced Graphene Oxide Electrodes from Cocoa Shell: Nanoarchitectonics Platform for Photoelectrocatalytic Detection of Methylene Blue". *Journal of Oleo Science.* **72** (12): 1133-1140. 10.5650/jos.ess23152.

[16] M. Nazhipkyzy, M. Yeleuov, S. T. Sultakhan, A. B. Maltay, A. A. Zhaparova, D. D. Assylkhanova, and R. R. Nemkayeva. (2022). "Electrochemical Performance of Chemically Activated Carbons from Sawdust

as Supercapacitor Electrodes". *Nanomaterials.* **12** (19). 10.3390/nano12193391.

[17] G. Manibalan, G. Murugadoss, P. Kuppusami, N. Kandhasamy, and M. R. Kumar. (2021). "Synthesis of Heterogeneous NiO Nanoparticles for High-Performance Electrochemical Supercapacitor Application". *Journal of Materials Science: Materials in Electronics.* **32** (5): 5945-5954. 10.1007/s10854-021-05315-9.

[18] T. H. Kim, J. H. Jeon, J. E. Kim, K. S. Kang, J. Yoon, C. S. Park, K. Jung, T. Han, H. Lee, H. Joo, and H. Lee. (2024). "Effect of α-FeOOH in KOH Electrolytes on the Activity of NiO Electrodes in Alkaline Water Electrolysis for the Oxygen Evolution Reaction". *Catalysts.* **14** (12). 10.3390/catal14120870.

[19] S. E. Siddiqui, M. A. Rahman, J. H. Kim, S. B. Sharif, and S. Paul. (2022). "A Review on Recent Advancements of Ni-NiO Nanocomposite as an Anode for High-Performance Lithium-Ion Battery". *Nanomaterials.* **12** (17). 10.3390/nano12172930.

[20] A. León, P. Reuquen, C. Garín, R. Segura, P. Vargas, P. Zapata, and P. Orihuela. (2017). "FTIR and Raman Characterization of TiO2 Nanoparticles Coated with Polyethylene Glycol as Carrier for 2-Methoxyestradiol". *Applied Sciences.* **7** (1). 10.3390/app7010049.

[21] P. K. Singh. (2021). "Thermo Gravimetric Analysis and FTIR Analysis of Electrochemically Synthesized Graphene Oxide (GO)/Reduced Graphene Oxide (rGO)". **1116** : 012003. 10.1088/1757-899X/1116/1/012003

[22] F. N. Ajjan, M. J. Jafari, T. Rębiś, T. Ederth, and O. Inganäs. (2015). "Spectroelectrochemical Investigation of Redox States in a Polypyrrole/Lignin Composite Electrode Material". *Journal of Materials Chemistry A.* **3** (24): 12927-12937. 10.1039/c5ta00788g.

[23] S. Mugundan, B. Rajamannan, G. Viruthagiri, N. Shanmugam, R. Gobi, and P. Praveen. (2014). "Synthesis and Characterization of Undoped and Cobalt-Doped TiO2 Nanoparticles via Sol–Gel Technique". *Applied Nanoscience.* **5** (4): 449-456. 10.1007/s13204-014-0337-y.

[24] N. D. Abazovic, M. I. Comor, M. D. Dramicanin, D. J. Jovanovic, S. P. Ahrenkiel, and J. M. Nedeljkovic. (2006). "Photoluminescence of Anatase and Rutile TiO2 Particles". *The Journal of Physical Chemistry B.* **110** (50): 25366-25370. 10.1021/jp064454f.

[25] L. S. Chougala, M. S. Yatnatti, R. K. Linganagoudar, R. R. Kamble, and J. S. Kadadevarmath. (2017). "A Simple Approach on Synthesis of TiO2 Nanoparticles and Its Application in Dye Sensitized Solar Cells". *Journal of Nano- and Electronic Physics.* **9** (4): 04005-1-04005-6. 10.21272/jnep.9(4).04005.

[26] W. Li, R. Liang, A. Hu, Z. Huang, and Y. N. Zhou. (2014). "Generation of Oxygen Vacancies in Visible Light Activated One-Dimensional Iodine TiO2 Photocatalysts". *RSC Advances.* **4** (70): 36959-36966. 10.1039/c4ra04768k.

[27] I. M. Joni, L. Nulhakim, and C. Panatarani. (2018). "Characteristics of TiO2 Particles Prepared by Simple Solution Method Using TiCl3 Precursor". *Journal of Physics: Conference Series.* **1080** : 012042. 10.1088/1742-6596/1080/1/012042.

[28] F. Davar, Z. Fereshteh, and M. Salavati-Niasari. (2009). "Nanoparticles Ni and NiO: Synthesis, Characterization and Magnetic Properties". *Journal of Alloys and Compounds.* **476** (1-2): 797-801. 10.1016/j.jallcom.2008.09.121.

[29] P. M. Kibasomba, S. Dhlamini, M. Maaza, C. P. Liu, M. M. Rashad, D. A. Rayan, and B. W. Mwakikunga. (2018). "Strain and Grain Size of TiO2 Nanoparticles from TEM, Raman Spectroscopy and XRD: The Revisiting of the Williamson–Hall Plot Method". *Results in Physics.* **9** : 628-635. 10.1016/j.rinp.2018.03.008.

[30] W. Chen, M. Gong, K. Li, M. Xia, Z. Chen, H. Xiao, Y. Fang, Y. Chen, H. Yang, and H. Chen. (2020). "Insight into KOH Activation Mechanism during Biomass Pyrolysis:

Chemical Reactions between O-Containing Groups and KOH". *Applied Energy.* **278**. 10.1016/j.apenergy.2020.115730.

[31] S. A. Al Kiey, R. Ramadan, and M. M. El-Masry. (2022). "Synthesis and Characterization of Mixed Ternary Transition Metal Ferrite Nanoparticles Comprising Cobalt, Copper and Binary Cobalt–Copper for High-Performance Supercapacitor Applications". *Applied Physics A: Materials Science and Processing.* **128** (6). 10.1007/s00339-022-05590-1.

[32] P. De, J. Halder, C. C. Gowda, S. Kansal, S. Priya, S. Anshu, A. Chowdhury, D. Mandal, S. Biswas, B. K. Dubey, and A. Chandra. (2022). "Role of Porosity and Diffusion Coefficient in Porous Electrode Used in Supercapacitors – Correlating Theoretical and Experimental Studies". *Electrochemical Science Advances.* **3** (1). 10.1002/elsa.202100159.

[33] C. H. Lin, L. Wang, S. T. King, J. Bai, L. M. Housel, A. H. McCarthy, M. N. Vila, H. Zhu, C. Zhao, L. Zou, S. Ghose, X. Xiao, W. K. Lee, K. J. Takeuchi, A. C. Marschilok, E. S. Takeuchi, M. Ge, and Y. K. Chen-Wiegart. (2021). "Probing Kinetics of Water-in-Salt Aqueous Batteries with Thick Porous Electrodes". *ACS Central Science.* **7** (10): 1676-1687. 10.1021/acscentsci.1c00878.